Meteorol. Z. (Contrib. Atm. Sci.), Vol. **30**, No. 3, 251–269 (published online March 26, 2021)

Variation of leading-edge-erosion relevant precipitation parameters with location and weather type

Anna-Maria Tilg[1*], Martin Hagen[2], Flemming Vejen[3] and Charlotte Bay Hasager[1]

[1]Technical University of Denmark, Department of Wind Energy, Roskilde, Denmark
[2]Deutsches Zentrum für Luft- und Raumfahrt (DLR), Institut für Physik der Atmosphäre, Oberpfaffenhofen, Germany
[3]Danish Meteorological Institute, Copenhagen, Denmark

(Manuscript received October 8, 2020; in revised form February 12, 2021; accepted February 14, 2021)

Abstract

Precipitation is a key driver of leading-edge erosion of wind turbine blades, which leads to a loss in annual energy production and high cost for repair of wind turbines. Precipitation type, drop size and their frequency are relevant parameters, but not easily available. Reflectivity-Rain Rate (Z-R) relationships as well as annual sums of rainfall amount and rainfall kinetic energy potentially could be used to estimate leading-edge erosion. Although Z-R relationships and amounts are known for several places, their spatial variation and dependence on weather types is unknown in the North Sea and Baltic Sea area. We analysed time series of multiple disdrometers located on the coast of the North Sea and Baltic Sea to characterize the variation and weather-type dependence of the Z-R relationship, precipitation type, rainfall amount and kinetic energy.

The Z-R relationship as indication for the mean drop-size distribution showed small variations within different locations, but had a large variability for specific, but rare weather types. Only the precipitation types snow and hail showed some tendencies of weather-type dependence. Rainfall amount and rainfall kinetic energy were higher for stations in the eastern part of the North Sea compared to the western part and the Baltic Sea. Highest values were related to advection from the West. Overall, variations with location and weather type were found. These results will need to be considered in leading-edge erosion modelling and site assessment.

Keywords: Z-R relationship, Rainfall kinetic energy, North Sea, Baltic Sea, Wind energy

1 Introduction

The demand for renewable energy is increasing worldwide. To satisfy this demand, many countries plan to increase the number of wind turbines offshore, where for example the European Union pursues the goal to increase their wind capacity offshore from 20 GW in 2019 to 450 GW in 2050 (Freeman et al., 2019). One of the challenges offshore is leading-edge erosion (LEE) (Verma et al., 2020). The material on the leading edge degrades due to the impact of particles, where precipitation particles (e.g. raindrops, hailstones) play a major role in the erosion process (Keegan et al., 2013; Slot et al., 2015). Negative consequences of LEE are the reduction of aerodynamic efficiency and a related loss in the annual energy production (AEP) (e.g. Sareen et al., 2014) as well as high costs for repair (Mishnaevsky, 2019). Detailed precipitation data are needed to predict LEE at offshore wind farm sites. The current study focuses on the spatial variation of relevant precipitation parameters for LEE in the North Sea and Baltic Sea where the majority of current and future offshore wind turbines in Europe are located.

*Corresponding author: Anna-Maria Tilg, Technical University of Denmark, Department of Wind Energy, Frederiksborgvej 399, 4000 Roskilde, e-mail: anmt@dtu.dk

The kinetic energy of the particles describes the available energy for erosion, which is a function of the particle's mass and velocity. Models and rain erosion tests show that the particle size is a key parameter, because different sizes cause different stresses in the material (Bech et al., 2018; Verma et al., 2020). The velocity of the impacting particles is the sum of the fall velocity of the particle and the speed of the wind turbine blade. The blade speed can be more than 10 times higher than the terminal fall velocity of a precipitation particle (Keegan et al., 2013). The cumulative sum of impacts on the blade is central in the damage models for material degradation (Slot et al., 2015). To summarize, the size and density of the precipitation particle as well its velocity and frequency are essential parameters for LEE. Fernandez-Raga et al. (2016) and Zambon et al. (2020) mention similar parameters to describe the soil erosion rate. Several statistical relationships between kinetic energy of rainfall and rain rate exist with respect to erosion (Tilg et al., 2020). Such an approach is more difficult for LEE as it cannot be assumed that the impact velocity is the (terminal) fall velocity of the precipitation particle but also depends on the speed of wind turbine blades, which is a function of wind speed and turbine type.

The precipitation type governs the density of the precipitation particles. For raindrops the density of water

($1\,g\,cm^{-3}$) is used and for hailstones values between 0.7 and $0.9\,g\,m^{-3}$ are assumed (Wang, 2013). Rain is the dominant precipitation type in the North Sea area, because of the temperate climate influenced by the Gulf Stream. Rain is also assumed to cause most of LEE. Tait et al. (1999) analyse annual and monthly rainfall amount in the North Sea using satellite data and find that precipitation conditions in the North Sea depend on land mass distribution but also on general circulation patterns. Furthermore, they show that in some years westerlies are less dominant than usual in the North Sea area and causing a different rain distribution for these years. Other precipitation types occur less frequently, but ice and hail can cause severe damage of the leading edges during short time (Macdonald et al., 2016; Letson et al., 2020). Therefore, it is important to consider the frequency for ice and hail as well. Hail occurs frequently in the Midwest of the USA where many wind turbines are in operation (Letson et al., 2020). Comparable observations on hail events in the North Sea area are not available. Punge and Kunz (2016) indicate that less hail is observed in Europe as compared to the USA.

The drop-size distribution (DSD) of raindrops is influenced by the drop formation process and collision with other raindrops during their way to the ground. The number of drops decrease with increasing diameter, which is often described with an exponential or gamma distribution. In situ measurements of DSD offshore are challenging due to harsh environmental conditions and missing infrastructure. There are only a few measurement campaigns that measured in situ DSD and precipitation type (e.g. Bumke and Seltmann (2012) and Klepp et al. (2018)). Bumke and Seltmann (2012) compare data from disdrometers installed at research vessels with data from disdrometers installed at land and find no significant difference in the DSD. The DSD determines other precipitation parameters like reflectivity (Z) and rain rate (R). While Z is proportional to the 6^{th} moment of the raindrop diameter and sensitive to large drops, R is proportional to the 3.67^{th} moment of the raindrop diameter and more sensitive to drops within the 1–3 mm range and the number of drops (Seo et al., 2010).

The Z-R relationship ($Z = A * R^b$) describes the empirical connection between these two precipitation parameters and is usually applied to convert Z measurements of weather radars into R. Especially the A-value, or prefactor, of the Z-R relationship indicates the presence (or absence) of large drops. In case the A-value is in the order of 300, convective rain with large drops can be expected. For an A-value around 50, it is drizzle (Hachani et al., 2017). According to Doelling et al. (1998), the b-value, or exponent, is of less importance, but also contains some information about the DSD. Hence, the Z-R relationship is another way to derive information of the DSD and could be an option for offshore precipitation characterisation. Doelling et al. (1998) present Z-R relationships for North Germany keeping the b-value fixed at 1.50. In contrast to Hachani et al. (2017), Kirsch et al. (2019) find higher A-values for stratiform rain than for convective rain, but a low variability of the b-value for both rain types analysing Micro Rain Radar data from North Germany.

Several studies show that the microphysics of precipitation and therefore DSD of rain vary with different atmospheric conditions (e.g. Hachani et al., 2017). Hence, there exist a lot of values for A and b for Z-R relationships, apart from the probably most used A-value of 200 and b-value 1.6 attributed to Marshall-Palmer (Ignaccolo and De Michele, 2020). A way to classify different atmospheric conditions is by a weather type (WT) or sometimes also called weather pattern. Fernandez-Raga et al. (2016) and Fernández-Raga et al. (2020) show that westerlies are dominating in Spain and that precipitation parameters and soil erosion patterns vary with WT. Aniol et al. (1980) compare Z-R relationships of four different WTs in South Germany. They find differences between the A- and b-values, where the values of the two most frequent WTs were quite similar. According to Piotrowicz and Ciaranek (2020), WT classification is divided into (i) morphological (defined by daily variation of selected meteorological parameters) and (ii) genetic (defined by synoptic and atmospheric circulation). Hidalgo and Jougla (2018) are describing a morphological WT classification, but several additional ones are existing. There are also several publications describing WTs based on genetic aspects like Linderson (2001). Bissolli and Dittmann (2001) define a WT classification for Germany also based on synoptic parameters, which should also be valid for the coastal parts of the North Sea and Baltic Sea. Hence, we assume that the combination of WT and Z-R can give valuable information about DSD at certain atmospheric conditions.

The aim of this study is to analyse the location- and weather-type dependence of Z-R relationships, precipitation types, rainfall amount and rainfall kinetic energy using disdrometer measurements at coastal stations of the North Sea and Baltic Sea and the mentioned weather-type classification of Bissolli and Dittmann (2001). We see Z-R relationships as another way to describe the DSD for estimating LEE. We assume that the Z-R relationships considering all measurements are quite similar for coastal stations at the North Sea and Baltic Sea, because Bumke and Seltmann (2012) found no considerable differences in DSD between land and sea. In contrast, we expect that Z-R relationships of specific WTs might vary considerable because of different atmospheric conditions. Furthermore, we investigate the variance of precipitation type, rainfall amount and rainfall kinetic energy for different WTs in the North Sea and Baltic Sea area. Following Tait et al. (1999), we expect that most precipitation is related to westerlies.

The paper is structured as followed: Chapter 2 gives an overview about the used data. Methods in Chapter 3 include the calculation of the analysed precipitation parameters as well as the description of the used weather-

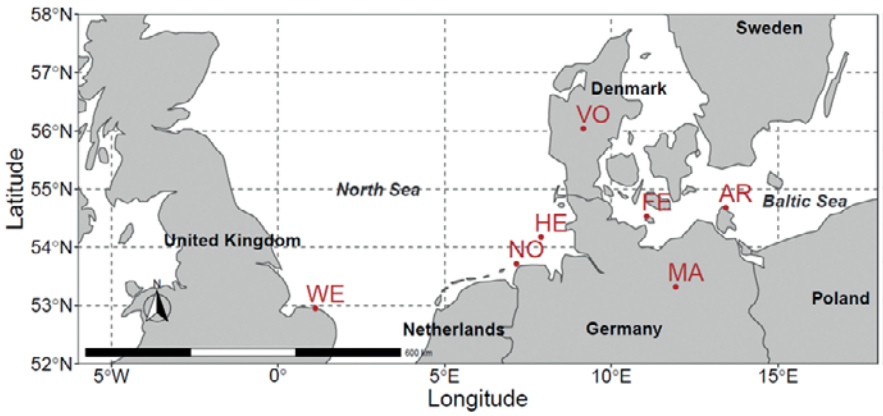

Acronym	Station	Country
AR	Arkona	Germany
FE	Fehmarn	Germany
HE	Helgoland	Germany
MA	Marnitz	Germany
NO	Norderney	Germany
VO	Voulund	Denmark
WE	Weybourne	United Kingdom

Figure 1: Map of investigation area including locations of analysed stations. The acronyms used for the stations are explained in the table.

type classification. The results in Chapter 4 present the location and weather-type dependence of the Z-R relationships, precipitation type, rainfall amount and rainfall kinetic energy for the analysed stations. The paper ends with a discussion in Chapter 5 and a conclusion in Chapter 6.

2 Data and quality control

For this study disdrometer measurements were analysed as they measure the number of precipitation particles as well as their size and fall velocity. These data also allow the classification of the precipitation particle type and the calculation of the parameters Z, R, rainfall amount and rainfall kinetic energy as they are integral parameters of the DSD. Data originated from the two disdrometer devices Thies Laser Precipitation Monitor (LPM), henceforward Thies, and Ott Parsivel^2, henceforward Ott. Both types generate a horizontal light plane by a laser between a transmitter and receiver. The number, size and fall velocity of precipitation particles is determined based on the amplitude and duration of the attenuation of the laser beam when a particle falls through it.

However, there are a few differences between the devices such as the wavelength of the used laser (Thies: 785 nm, Ott: 650 nm) and the housing of the sensors. Thies has 22 diameter (0.1875 mm to $\geq$ 8.000 mm) and 20 velocity (0.100 m s^{-1} to 15.000 m s^{-1}) classes with varying class width and hence 440 classes in total to refer measured precipitation. Ott has 32 diameter (0.062 mm to 24.500 mm) and 32 velocity (0.050 m s^{-1} to 20.800 m s^{-1}) classes with varying class width and hence 1024 classes in total. For both devices the mean value of the class is given. The performance of both devices has been focus of several studies (e.g. Frasson et al., 2011; Raupach and Berne, 2015; Johannsen et al., 2020). Angulo-Martínez et al. (2018) find that Thies measures more small drops while Ott measures more large drops. According to Fehlmann et al. (2020) the distinction of rain and snow of Thies is similar to the measurements of the two-dimensional video disdrometer (2DVD) (Kruger and Krajewski, 2002)

Measurements from 13 different stations in three different countries have been available. All of them are at the coast or close to the coast of the North Sea and Baltic Sea where many offshore wind turbines are installed (Fig. 1):

- Denmark: Data from six Danish stations were provided by Danmarks Tekniske Universitet (DTU) and Danmarks Meteorologiske Institut (DMI) and included six datasets measured with Ott in Horns Rev 3 (offshore wind farm), Hvide Sande, Risø, Rødsand (offshore wind farm), Thyborøn, Voulund and one dataset measured with Thies in Voulund. In Voulund the device was changed from Thies to Ott in 2018.
- Germany: Data from six German stations was provided on request by Deutscher Wetterdienst (DWD) and included datasets measured with Thies in Arkona, Bremerhaven, Fehmarn, Helgoland, Marnitz and Norderney.
- United Kingdom (UK): Data measured with Thies in Weybourne in the UK was available via the Natural Environment Research Council's Data Repository for Atmospheric Science and Earth Observation, also known as CEDA archive (Natural Environment Research Council et al., 2019).

Quality control of the disdrometer data was done in three steps. Data were checked related to (i) non-precipitation data by using internal quality parameters, (ii) correct precipitation type comparing surface synoptic observation (SYNOP) code from the disdrometer with the probability for specific precipitation type using temperature and relative humidity and (iii) limits of size and terminal velocity of raindrops. The necessary temperature and relative humidity data were available via the Open Data Server from DWD for the German stations, via CEDA for the UK station (Bandy, 2002) and on request for Danish stations. Due to high amounts of missing values and data quality issues only the seven stations Arkona, Fehmarn, Helgoland, Marnitz, Norderny, Voulund (time series with Thies) and Weybourne were used for further analysis. The disdrometer at station Risø was quite sheltered, as the angle between the disdrome-

ter and the surrounding obstacles was equal or above 30° in most directions. Hence, this station was also excluded from the analysis. For further information about the quality control, the reader is referred to the Appendix.

3 Methods

The applied weather-type (WT) classification is based on Bissolli and Dittmann (2001). The temporal resolution of this WT classification is one day, where values of an operational weather analysis and forecasting system at 12 UTC are used for classification. As this WT classification was developed with focus on Germany, DWD provides the time series of WTs back to 1979 free of charge on its website. In this study, we used this free available time series of WTs of DWD.

Bissolli and Dittmann (2001) use five letters to describe the WT and the related atmospheric conditions. The first two letters describe the advection direction (horizontal wind direction in 700 hPa), the following two letters describe the cyclonality in 950 and 500 hPa and the last letter the humidity (precipitable water in the troposphere above or below to the long-term mean of 1979 to 1996). There are following options for each of the letters:

- Advection: NE (northeast), SE (southeast), SW (southwest), NW (northwest), XX (no prevailing wind direction in case less than two thirds of the grid points have wind from the same direction)
- Cyclonality: anticyclonic (A; large-scale circulation in clockwise direction), cyclonic (C; large-scale circulation in anti-clockwise direction)
- Humidity: wet (W), dry (D)

All possible combinations lead to a total number of 40 weather types (WTs). For example, the WT with the abbreviation NWAAW describes an advection from northwest (NW), the cyclonality in 950 and 500 hPa is anticyclonic (AA) and a wet atmosphere (W). The WT with the abbreviation SECAW describes an advection from southeast (SE), the cyclonality in 950 hPa is cyclonic (C), the cyclonality in 500 hPa is anticyclonic (A) and a wet atmosphere (W).

Quality controlled disdrometer data with a temporal resolution of 1 minute were used to calculate LEE relevant precipitation parameters.

The relationship between Z and R is usually described with a power law:

$$Z = A * R^b \tag{3.1}$$

with A as the prefactor and b as the exponent. Both, Z and R, depend on the DSD, often described with a drop concentration $N(D_i)$ ($m^{-3}\,mm^{-1}$). For this study $N(D_i)$ was calculated using the parameterization approach from Ulbrich and Atlas (1998) considering only rain, where

$$N(D_i) = N_0 * D_i^{\mu} * e^{-\Lambda D_i} \tag{3.2}$$

with D_i being the mean drop diameter in class i (mm), N_0 as intersect ($m^{-3}\,mm^{-1}$), μ as shape factor, and Λ as slope (mm^{-1}). It is a further quality control step, because some measured data had no gamma distribution and could not be fitted with this approach, probably because the measurements did not originate from rain. The rain rate R ($mm\,h^{-1}$) was then calculated based on Seo et al. (2010):

$$R = 6 * \pi * 10^{-4} * \sum_i N(D_i) * D_i^3 * v_t * \Delta D_i \tag{3.3}$$

with v_t being the terminal fall velocity based on Atlas et al. (1973) ($m\,s^{-1}$) and ΔD_i being the diameter interval (mm). The terminal fall velocity based on Atlas et al. (1973) is calculated as follows:

$$v_t = 9.65 - 10^3 * e^{-600 * D_i} \tag{3.4}$$

The reflectivity Z ($mm^6\,mm^{-3}$) was calculated as follows (Seo et al., 2010):

$$Z = \sum_i N(D_i) * D_i^6 * \Delta D_i \tag{3.5}$$

To determine the A- and b-value of the Z-R relationship, a nonlinear least-squares estimate with Z as independent variable of the following nonlinear model, derived from equation (3.1), was performed:

$$R = 10^{(b^* \log(Z) - A^*)} \tag{3.6}$$

This was done using R 4.0.1 (R Core Team, 2020) and the function nls in the stats package. According to Krajewski and Smith (1991) and Alfieri et al. (2010) a linear regression estimation using the log-scale of R and Z would lead to biased values of the A- and b-value. For each station a Z-R relationship was fitted using all 1-minute measurements, independent of the WT classification or event. Furthermore, separate Z-R relationships were fitted using only Z and R values related to the specific WT. To calculate the Root Mean Square Error (RMSE) between measured R and R based on the fitted Z-R relationship, 75 % of the data were used for fitting the A- and b-value, the remaining 25 % for an independent calculation of the error (training and validation dataset). Only measurements with $R > 0.1\,mm\,h^{-1}$ were considered in the training process. The choice of this R threshold influences the fitted A- and b-values as well (Verrier et al., 2013). If the number of training values was below 50, no fitting was done. Therefore, not all stations had Z-R relationships for all WTs. The RMSE is defined as:

$$RMSE = \frac{1}{n}\sqrt{\sum_i (y_i - o_i)^2} \tag{3.7}$$

where y is the calculated R, o the measured R and n the number of pairs. For the calculation of the RMSE it was assumed that the measured R was the calculated R

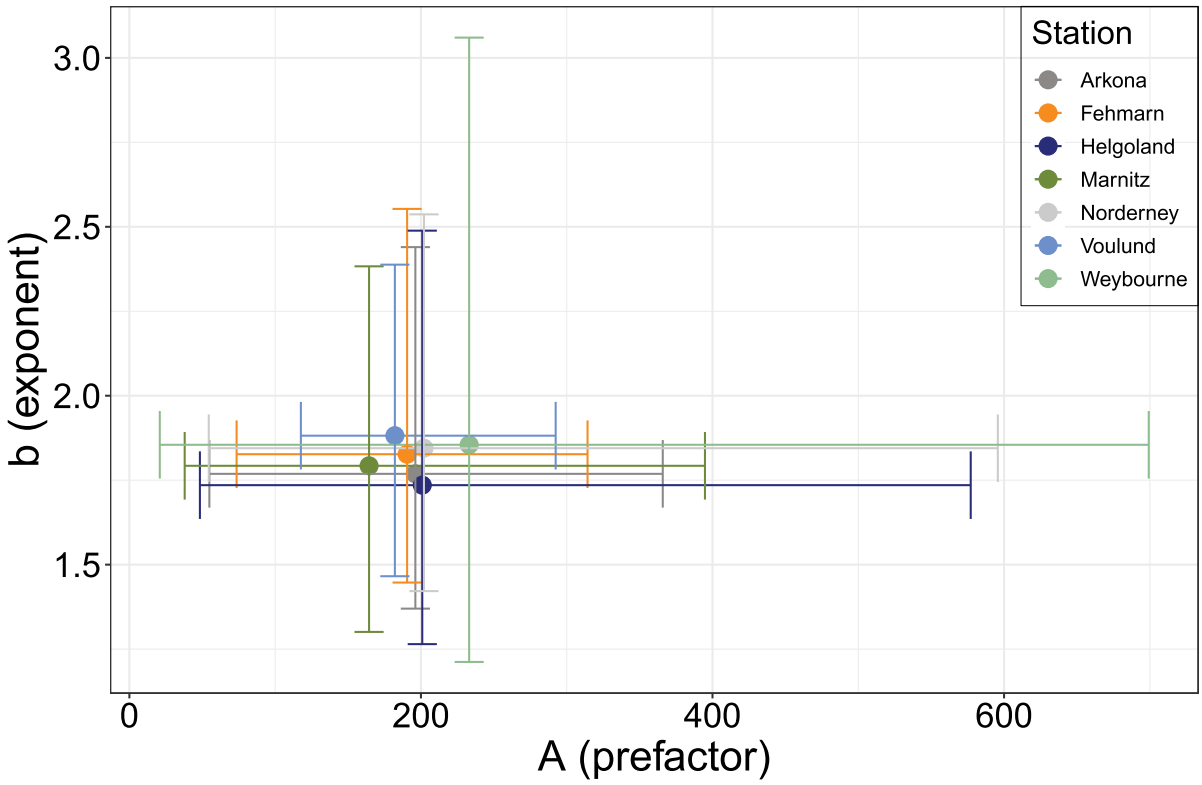

Figure 2: Fitted A- and b-values of the Z-R relationship for all stations. The points represent A and b fitted using all 1-minute measurements. The bars indicate the range of A and b fitted with measurements taken during specific weather types.

based on the parameterized DSD calculated with equation (3.3).

Rainfall amount (AMT; mm) is the volume of all measured raindrops and was calculated using disdrometer data and following equation:

$$AMT = \frac{1}{A} * \frac{\pi}{6} * \sum_i n_i * D_i^3 \tag{3.8}$$

where A is the measuring area (m^2) and n_i the number of drops. To get a mean annual rainfall amount for each station although having incomplete years, following procedure was applied: (i) Sum of rainfall amount over whole available time period, (ii) Number of days between first and last observation, (iii) Division of overall rainfall amount by number of observation days and multiplication of this value with 365 to get mean annual rainfall amount. The annual mean value should not be influenced that much by gaps, because only stations with a low amount of missing values were selected.

Rainfall kinetic energy per area (KE, $J\,m^{-2}$) is based on Petrů and Kalibová (2018):

$$KE = \frac{1}{A}\frac{\rho * \pi}{12} \sum_i \sum_j n_{ij} * D_i^3 * v_j^2 \tag{3.9}$$

where ρ is the water density ($kg\,m^{-3}$). For this study the fall velocity of the raindrops measured by the disdrometer was used for the KE calculation. Hence, only the KE provided by rainfall was analysed. To calculate the mean annual KE, the same procedure was applied as for the mean annual rainfall amount.

A probability was calculated to investigate the frequency that for a certain WT precipitation was registered or a certain precipitation type occurred:

$$P = \frac{\#measurements\ fulfilling\ requirements}{\#measurements} \tag{3.10}$$

4 Results

4.1 Z-R relationship

The A- and b-values of the location-specific Z-R relationship were fitted using quality controlled 1-minute disdrometer data and considering only rain. To evaluate the dependence on WTs, separate A- and b-values were fitted using only data measured during the specific WT. Fig. 2 shows the distribution of the fitted A- and b-values for each location. The points represent the A- and b-values based on all measurements independent of the WT. The A-values vary between 164 (Marnitz) and 233 (Weybourne). The higher (lower) A-value might be due to slightly larger (smaller) mean drop diameters at Weybourne (Marnitz). The b-values varied between 1.74 (Helgoland) and 1.88 (Voulund) and were quite similar. The horizontal and vertical bars indicate the range of A- and b-values of the analysed WTs. The station Weybourne had the largest spread of A- and b-values with A-values between 21 and 699 and

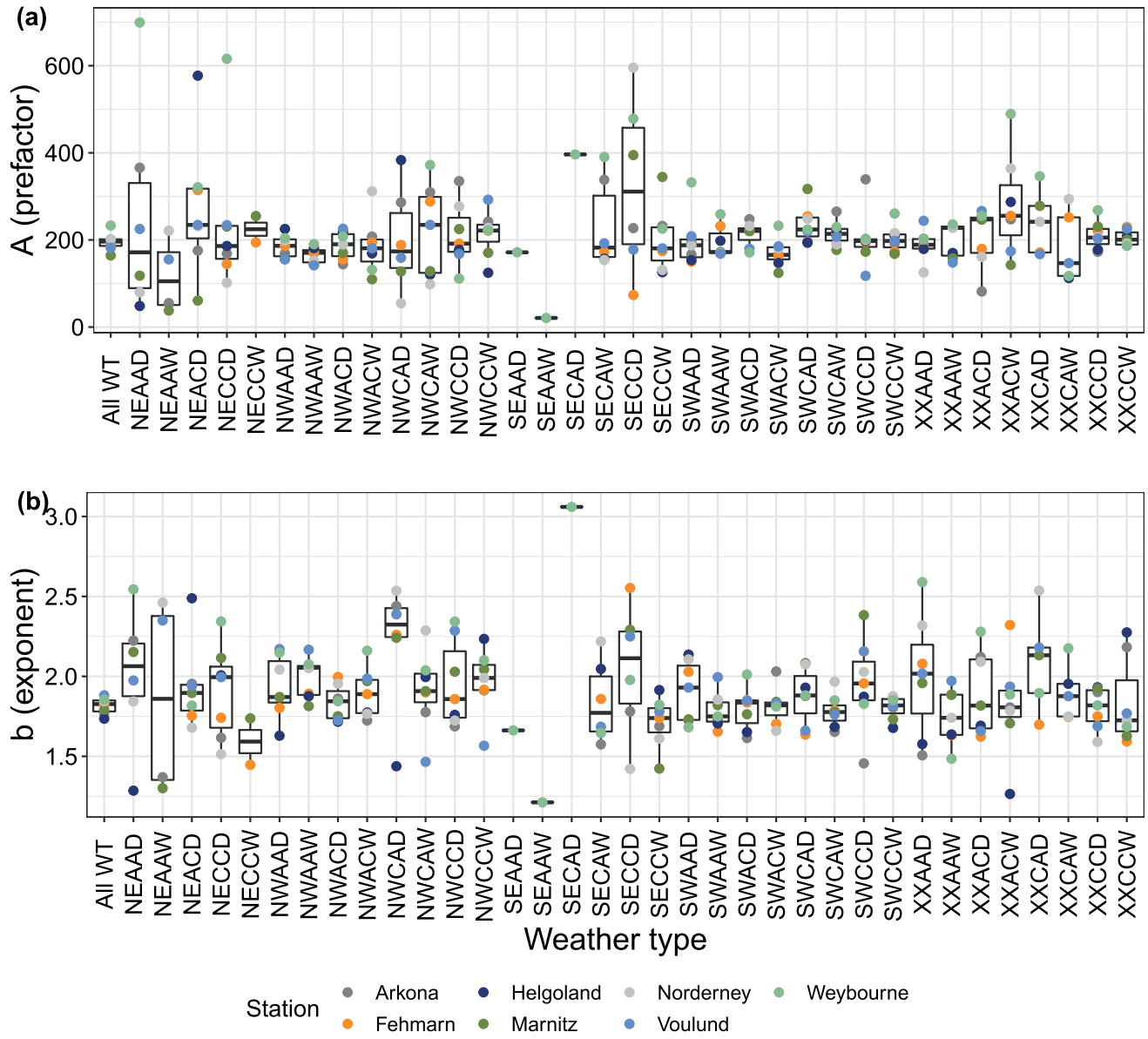

Figure 3: Weather-type (WT) dependence of (a) A-values and (b) b-values. Box-whiskers plots show the variability of the values for each WT. The box is represented by the 1st and 3rd quartile and the whiskers by 1.5 times the interquartile range above and below the 1st and 3rd quartile. Values above or below the whiskers are outliers. The coloured points represent the value of the specific station. The WT is described with five letters, where the first two letters describe the advection direction (NE, NW, SE, SW, XX = no prevailing direction), the following two letters describe the cyclonality in 950 and 500 hPa (A(nticyclonic), C(yclonic)) and the last letter the humidity index (W(et), D(ry)).

b-values between 1.21 and 3.05. The bars of the remaining stations cover a similar range of values. The A- and b-values of station Fehmarn for WT NEAAD were not considered in Fig. 2 and Fig. 3, because the A-value with 2997 and the b-value with 3.15 were much higher compared to the other fitted values. These high values might be caused by the fact that only R values below 1 mm h^{-1} were measured during this WT. All fitted A- and b-values can be found in the Appendix.

The WT-dependence of A and b at the different locations is investigated more deeply next. Fig. 3 shows a box-whiskers plot of the A- and b-values for each WT. The box represent the values within the first and third quartile and with the thick line being the median. The whiskers are 1.5 times the interquartile range (IQR) above the third quartile and below the first quartile, where the interquartile range is the difference between the third and first quartile. Values above or below the whiskers are classified as outliers. That means that a small box and short whiskers indicate a small variability of the values, while a large box and large whiskers indicate a large variability. The box-whiskers plots were overlaid with the WT-specific A- and b-values of the stations. For five WTs (SEACD, NEACW, SEACW, NECAD, NECAW) no station had the required number of 50 measurements to fit the Z-R relationship. For three

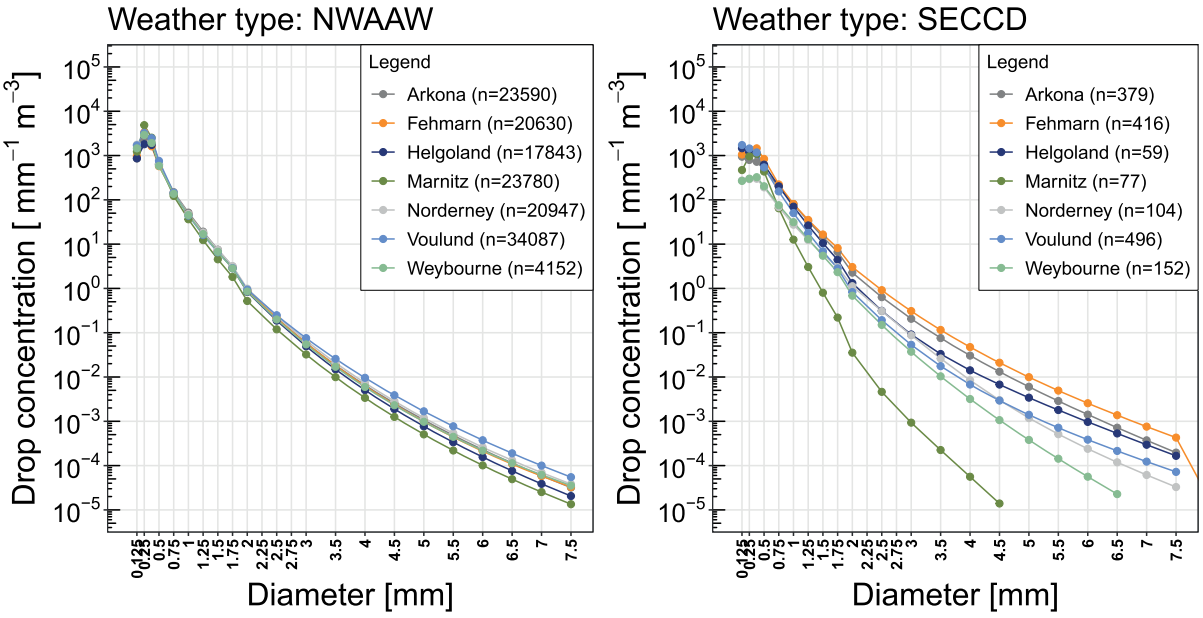

Figure 4: Mean 1-minute parameterized drop concentration for the weather types (left) NWAAW (advection from Northwest, anticyclonality in 950 and 500 hPa, wet humidity index) and (right) SECCD (advection from Southeast, cyclonality in 950 and 500 hPa, dry humidity index). The number of considered 1-minute values is given in the parenthesis next to the station name.

WTs (SEAAD, SEAAW and SECAD) it was only station Weybourne that had enough measurements to fit the A- and b-values of the Z-R relationship.

For 28 out of 32 WTs the median of the A-values had a value of 200 +/− 50. Two WTs (NEAAW and XXCAW) had a median below 150 and two WTs (XXACW and SECCD) had a median above 250. Higher (lower) A-values indicate that a higher (lower) amount of large raindrops was observed during these WTs, maybe related to more (less) convective rain. Although the similar median values support a small variability between WTs, the difference between the highest and lowest A-value of each WT showed a large variability between the stations for some specific WTs. While 11 out of 32 WTs had a maximum-to-minimum difference below 100, four WTs (NEAAD, NEACD, NECCD and SECCD) had a difference above 500. These high variations would lead to the assumption that the underlying DSD of the stations was quite different for the same WT.

The majority of the median b-values were within 1.90 +/− 0.30. One WT (NWCAD) had a median b-value above 2.20, while one WT (NECCW) had a median b-value below 1.70. Equal to the A-value, the maximum-to-minimum difference of the b-values of the stations was quite high for some WTs. The difference included values between 0.20 for WT SWCCW and 1.86 for WT NEAAD.

A comparison of WTs with a high variation for different locations showed that they (i) often had a high variability of A- and b-value (e.g. WTs NEAAD or SECCD) and (ii) were often fitted with the minimal number of 50 observations or only slightly more. The low number of observations leads to the assumption that the specific WT occurred rarely. This will be investigated further in the next chapter. To summarize, the A- and b-values varied to a certain degree between the locations for all WTs, where only for a few WTs the values varied considerable between different locations.

The variability of A- and b-values can be compared with the variability of the mean DSD, as Z and R depend on the DSD. As an example, Fig. 4 shows the mean 1-minute parameterized DSD of the WTs NWAAW and SECCD. The parameterization of the DSD was done following the steps described in Ulbrich and Atlas (1998). While the WT NWAAW had a low variability of A- and b-values between the stations, SECCD had one of the largest variabilities of A- and b-values. The drop concentrations in Fig. 4 showed a similar pattern. For the WT NWAAW the difference between the drop concentrations of the stations was small. In contrast, for the WT SECCD there were quite some differences between the drop concentrations at all diameters. The number of 1-minute observations available to calculate the A- and b-values were much higher for the WT NWAAW (min. 4152) compared to WT SECCD (max. 496).

A performance indication of the fitted A- and b-values is the error between measured and calculated R. In Fig. 5 the distribution of the Root Mean Square Error (RMSE) between the measured R and the calculated R for all WTs is shown using box-whiskers plots. The RMSE was calculated for each station and WT using the validation dataset. The fitted A- and b-values and the A- and b- value based on Marshall-Palmer, respectively, were used to calculate R. The applied Marshall-Palmer values were: A = 200, b = 1.6 (Marshall et al., 1955). The median of the RMSE values, indicated by the black thick line in Fig. 5, was lower for R using WT dependent A- and b-values compared to the R

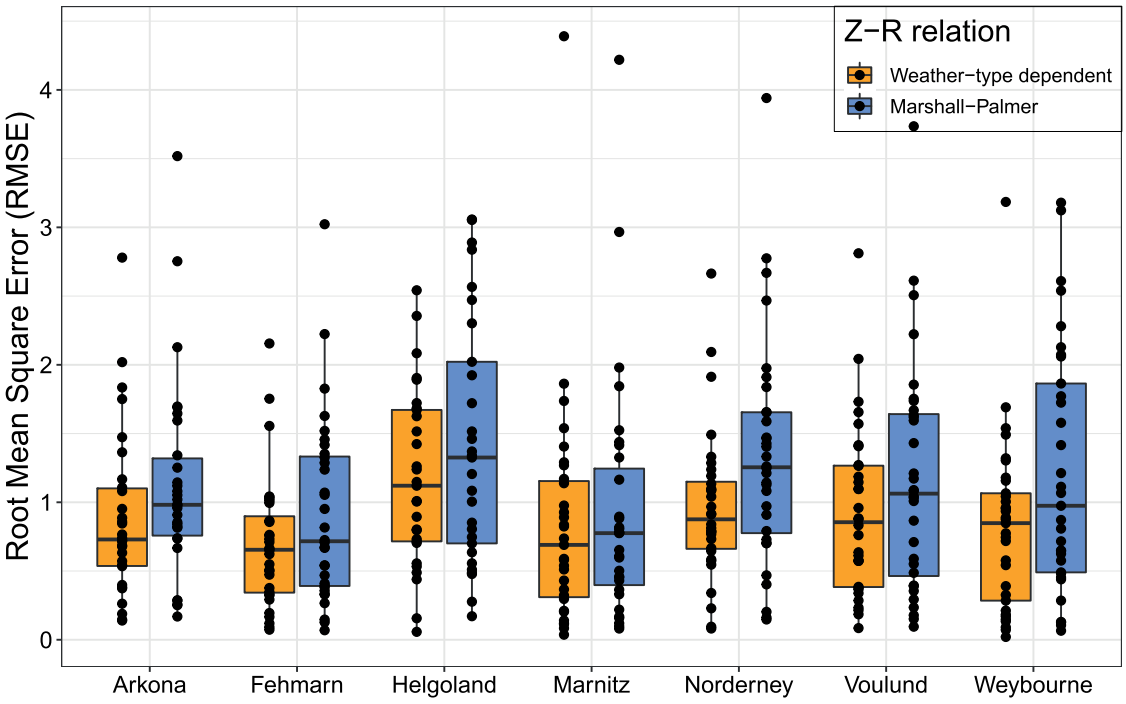

Figure 5: Distribution of the Root Mean Square Error (RMSE) between measured rain rate and calculated rain rate for 40 weather types (WT). For the orange boxplots WT-dependent A- and b-values were used. For the blue boxplots the values A = 200 and b = 1.6 based on Marshall-Palmer were used. Black dots are the RMSE values of the different WTs.

using Marshall-Palmer. The median RMSE varied between 0.64 (Marnitz) and 1.06 (Helgoland) using the fitted A- and b-values and between 0.71 (Fehmarn) and 1.27 (Helgoland) using Marshall et al. (1955). Overall, the lower error for R calculated with WT-dependent A- and b-values indicates a higher accuracy compared to R values calculated with a standard Z-R relationship.

4.2 Dependence of precipitation probability on weather type

To find WTs with the highest precipitation probability considering all precipitation types, for each station the cumulative number of minutes with precipitation was related to the cumulative number of minutes with precipitation for a specific WT (Fig. 6). It was found that only two WTs (SWAAW, NWAAW) had probabilities above 0.14 to observe precipitation. For another three WTs (NWACD, SWCAW and SWCCW) the probability was between 0.093 and 0.14. The probability to observe precipitation of any kind in one of these five WTs was between 0.44 (Weybourne) and 0.56 (Helgoland). For comparison, WTs with a large spread of fitted A- and b-values of the Z-R relationship (e.g. NEAAD and SECCD) had a probability below 0.01. Low probabilities or a complete absence of precipitation was observed for five WTs (SEAAW, NEACW, SEACW and NWCAD, NECAW). For one WT (NECAD) no station observed any precipitation during the analysed time period. This analysis shows that precipitation observations were dominated by WTs with SW and NW advection.

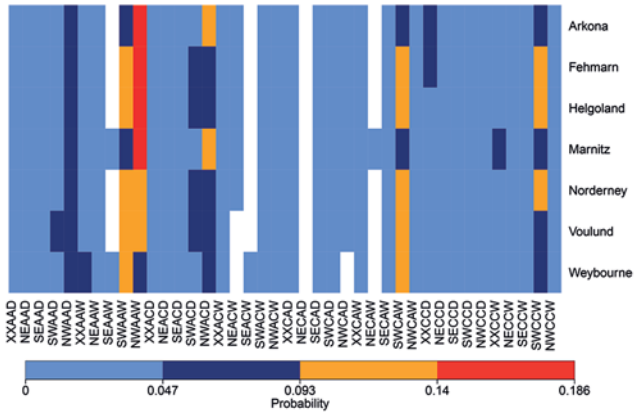

Figure 6: Probability to observe precipitation and its dependence on the weather type. Probabilities above zero are represented by the given colour scale. White areas represent a probability of zero.

4.3 Distribution and weather-type dependence of precipitation types

As mentioned, occurrence of hail (and ice) can be harmful for LEE. Therefore, it is necessary to investigate the distribution of different precipitation types on the overall time with precipitation. Table 1 gives an overview of the cumulative number of minutes with precipitation, which depends on the length of the available time series, and its distribution over the five different precipitation groups. The precipitation type rain was observed most often with a percentage between 90.03 % (Arkona) and 95.89 % (Helgoland). The precipitation type snow was observed

Table 1: Minutes with precipitation and distribution over the five defined precipitation groups.

Station	# Minutes with precipitation	% Rain/drizzle	% Mixed rain/snow	% Snow	% Ice	% Hail
Arkona	218984	90.03	1.07	8.57	0.30	0.03
Fehmarn	232254	92.40	1.13	6.16	0.26	0.05
Helgoland	188579	95.89	1.13	2.22	0.69	0.07
Marnitz	225075	90.50	1.31	7.68	0.48	0.03
Norderney	250887	94.77	0.90	2.62	1.60	0.11
Voulund	412218	91.11	0.95	7.41	0.47	0.06
Weybourne	127603	95.83	0.38	2.45	1.29	0.05

second most and between 8.57 % (Arkona) and 2.22 % (Helgoland) of the analysed precipitation time. Except for Norderney, these two precipitation types were observed in more than 98 % of the time with precipitation. The remaining precipitation types, mixed (rain and snow at the same time), ice and hail occurred between 1.60 % (Norderney, ice) and 0.03 % (Arkona, hail) of the time. The stations Norderney and Weybourne had in comparison to the other stations a high percentage of the precipitation type ice.

To investigate the dependence of the precipitation type on the WT, the probability between the number of minutes with precipitation for one specific WT and the number of minutes with a specific precipitation type for one specific WT was calculated. Fig. 7 shows the probability to observe a specific precipitation type depending on the WT.

For the precipitation types mixed, ice and hail single high probabilities compared to rain and snow were observed. For the precipitation types rain, snow and hail some dependence on the WT can be seen in Fig. 7. Some WTs with advection from east and no prevailing advection direction, respectively, had a lower probability of rain but a higher probability of snow. The precipitation type hail occurred mostly related to WT with advection from NW or SW.

As already shown in Table 1, the probabilities to measure rain or snow were highest. Hence, it is not surprising that most WTs had the highest probability to observe rain. Apart from 0, the lowest probability was 0.077 (Marnitz, SEACD) and multiple stations and WTs had a probability of 1. A probability of 1 means in this connection that precipitation occurred only as rain and no other precipitation type was observed during this WT.

As the top right plot in Fig. 7 shows, for two WTs (NEACD, XXCAD) half or more of the stations had a probability higher than 0.5 to observe snow. This high probability means that in case this WT was observed during half of the time or more the registered precipitation type was snow. For the WT SEACD the station Voulund had even a probability of 1 to observe snow.

In case of the precipitation type mixed (centre left in Fig. 7), the station Helgoland is outstanding. In this case, 19 out of 60 minutes with precipitation during WT SEACD were classified as mixed and led to a probability of 0.317. The remaining probabilities to observe mixed were below 0.115.

The probability to observe precipitation in form of ice was except for the station Arkona (WT XXACW) below 0.147 (centre right in Fig. 7). The probability of 0.375 at station Arkona for the mentioned WT was caused by the ratio of 8 minutes precipitation to 3 minutes with ice.

According to the bottom plot in Fig. 7, the probability to observe hail was below 0.004 except for the station Voulund (WT NWCAD). The probability of 0.008 at Voulund was caused by the relation of 7 minutes with hail to 856 minutes with precipitation in total.

It is important to note that the number of ice and hail observations were low, especially for rare WTs. This factor must be considered when interpreting the probability values.

4.4 Weather-type dependence of annual rainfall amount and rainfall kinetic energy

For a siting assessment of wind turbines related to LEE, not only information of the DSD might be relevant but also cumulative values of rainfall amount or rainfall kinetic energy (KE). Fig. 8 shows the mean annual rainfall amount and KE per WT. Only rain was considered for both parameters and KE was calculated using the measured fall velocity of the raindrops. As the analysed time series had a different length, a mean daily value was calculated and multiplied with 365 to get the mean annual rainfall amount and KE, respectively.

The mean annual values were higher at stations close the eastern part of the North Sea (Helgoland, Norderney and Voulund) with values above 700 mm / 8500 J m^{-2}. In contrast, stations at or close to the Baltic Sea or the western part of the North Sea (Arkona, Fehmarn, Marnitz and Weybourne) had values below 550 mm / 7500 J m^{-2}. Interestingly, Weybourne had a higher KE although having a similar rainfall amount as the other stations. This example shows that the ratio between rainfall amount and KE was not the same for all stations. The difference is caused by a higher number of larger raindrops (with higher fall velocity) in Weybourne as already indicated by the higher fitted A-value in Section 4.1.

The absolute rainfall amount per WT varied between the lower threshold of 0.01 mm and 113 mm (Voulund, SWAAW). Five WTs (SWAAW, NWAAW, SWACD,

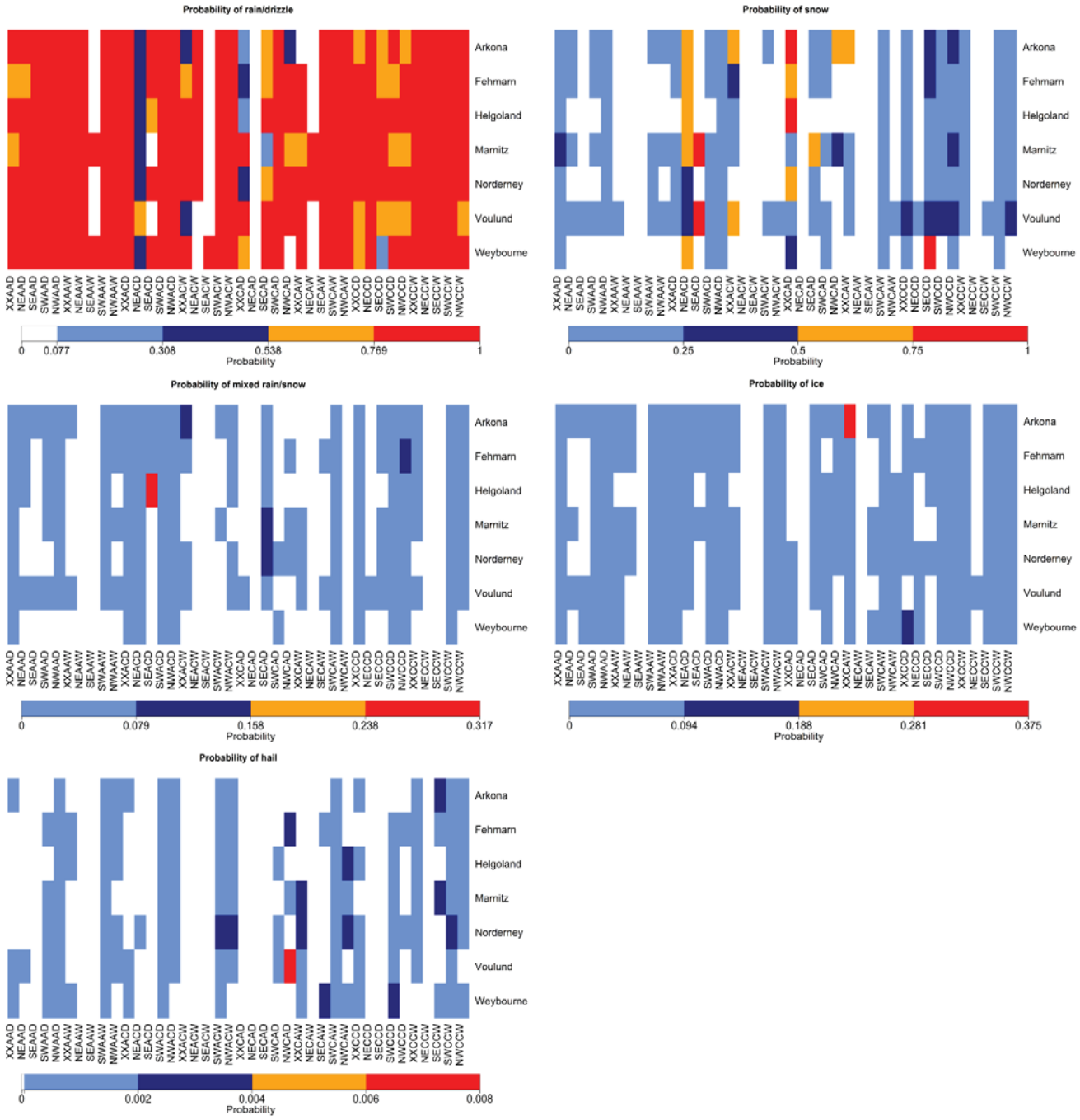

Figure 7: Probability to observe (top left) rain/drizzle, (top right) snow, (centre left) mixed, (centre right) ice and (bottom left) hail depending on the weather type. Probabilities above zero are represented by the given colour scale. White areas represent a probability of zero.

SWCAW and SWCCW) registered rainfall amounts above 84 mm. Furthermore, these five WTs provided together between 50 (Marnitz) and 58 % (Voulund) of the annual rainfall amount at all stations. These WTs were also WTs with the highest probability to be observed (see Fig. 6). The pattern is similar for KE, where values up to 1480 J m^{-2} (Voulund, SWAAW) were calculated for a single WT. Four WTs (SWAAW, SWACD, SWCAW, SWCCW) had values above 1110 J m^{-2} and contributed between 40 (Arkona) and 53 % (Weybourne) to the overall KE per station. For six WTs (SEAAD, SEAAW, NEACW, SEACW, NECAD, NECAW) the majority or all of the stations registered no or negligibly rainfall amount and KE, respectively. Hence, both parameters were dominated by rain related to advection from Southwest (SW). Furthermore, the comparison shows that a similar rainfall amount can lead to different values of KE.

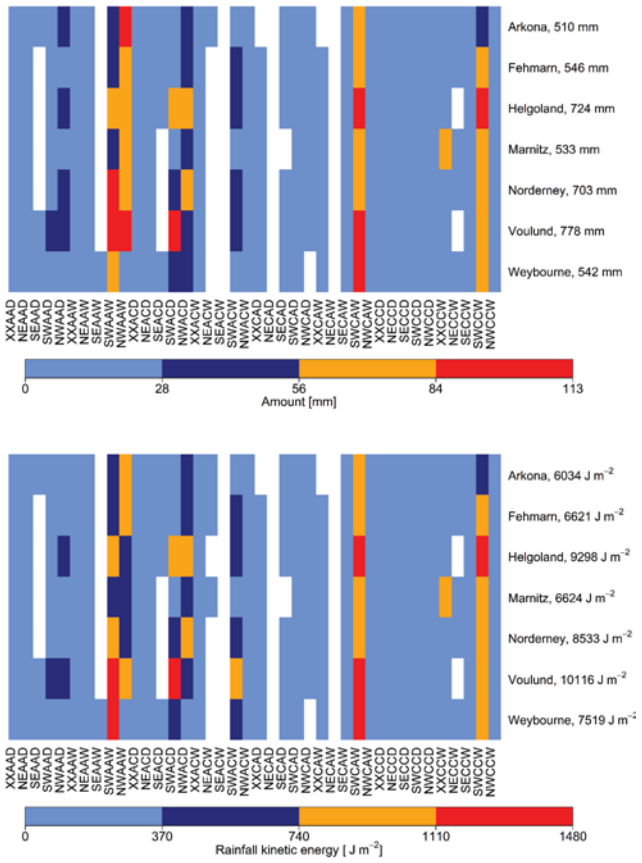

Figure 8: Mean annual (top) rainfall amount and (bottom) rainfall kinetic energy (KE) registered per weather type. Values above 0.01 mm / 0.01 J m^{-2} are represented by the given colour scale. White areas represent no rainfall amount / KE or values below the threshold. The mean cumulative value for each station is given next to the station name.

5 Discussion

The erosion of the leading edges of wind turbine blades is caused by the impact of hydrometeors. To estimate spatial variations of precipitation parameters relevant for LEE, several parameters like Z-R relationship, precipitation type, rainfall amount and rainfall kinetic energy were analysed regarding their variation with location and weather type (WT). We showed that the Z-R relationship of seven analysed stations was similar but varied considerable for some WTs. WTs with advection from NW and SW were most dominant and provided the majority of annual rainfall amount and rainfall kinetic energy. Rain and snow were observed around 98 % of the time, precipitation in form of ice and hail during the rest of the time.

All shown results were based on measurements with the disdrometers Thies LPM and Ott Parsivel^2. Angulo-Martínez et al. (2018) report that the Thies measures more small raindrops than Ott, while Ott tends to underestimate the fall velocity compared to a theoretical fall velocity model and Thies. They show that this behaviour has implications for all DSD-dependent precipitation parameters like rain rate. As the real ground truth of precipitation is not known, it is difficult to quantify the uncertainty of both sensors in absolute numbers. Raupach and Berne (2015) propose an algorithm to correct the measured drop fall velocity of an Ott using data of a two-dimensional video disdrometer (2DVD). According to them, this correction algorithm is applicable to different disdrometer types and locations and increases the accuracy of DSD-based precipitation parameters. Adirosi et al. (2018) conclude that for establishing long-term radar algorithms the disdrometer type plays a smaller role than for analysing the microphysics of a single event. As the focus of the above presented results was on long-term values, their conclusion are positive news for this study.

Despite the applied quality control of the disdrometer data, it was not possible to avoid having non-precipitation particles in the applied DSD. In case of the Z-R fitting procedure, the parameterisation of the DSD for calculating rain rate and reflectivity, worked as additional quality control step. In case of the quality control of the precipitation type only the plausibility of observing a specific type was investigated, but not the plausibility of precipitation itself. The latter would have only been possible using data from other sensors, which were not available for all stations. Such non-precipitation particles can led to some unrealistic results. An additional problem related to the precipitation type is that Thies and Ott store only the highest WMO SYNOP value, although different WMO SYNOP values and therefore precipitation types can occur at the same time (e.g. rain and hail during a thunderstorm). Furthermore, precipitation type statistics from disdrometers give only a very local impression especially in relation to ice or hail. In general, events with hail are not frequent and often only local. Hence, it is not very likely to observe hail within the small measurement area of the disdrometer (0.0054 m^2 for Ott and 0.00456 m^2 for Thies). To confirm such results, observations should be validated with human observers or data from dual-polarization weather radars.

Not only non-precipitation particles in the dataset, but also the duration of the time series, the related frequency of specific WT and occurrence of extreme values (low or high) can lead to uncertainties in the results. For example, in case of the station Fehmarn a lot of low R values were measured during a WT with low probability (NEAAD) and caused A- and b-values varying strongly from the other values. Doelling et al. (1998) mention that small samples can produce a statistical variability that could be wrongly interpreted as natural variability. Hence, one needs to be cautious in analysing and interpreting data from infrequent WT and precipitation types. According to Krajewski and Smith (1991) more than 10000 independent data samples are required to get valid estimates of A- and b-values. However, as the time periods of the analysed disdrometer measurements were short from a climatological aspect, this requested number of data samples could not be fulfilled in this investi-

gation. The low number of observations influenced also the probability of observing a specific precipitation type. For example, high probabilities of ice or hail calculated for rare WTs must be interpreted with caution and might not always reflect the climatological conditions.

A drawback from the applied weather-type classification is that the WT is assigned every day at 12 UTC. It can happen that the synoptic conditions changed before or after that time and would require allocating measured precipitation to another WT.

The range of fitted A-values of all stations varied between 164 and 233 using all 1-minute measurements independent of the WT and was therefore around the frequently used A-value of 200 (Marshall et al., 1955). The fitted b-values (1.74–1.88) are slightly above the frequently used b-value of 1.6 (Marshall et al., 1955). While Marshall and Palmer (1948) publish an A-value of 220 and a b-value of 1.60, Marshall et al. (1955) mention revised values of $A = 200$ and $b = 1.6$ for the Z-R relationship. The low variation between the different locations follows the assumption based on Bumke and Seltmann (2012) who state a low variation of DSD between sea and land considering data from the North Sea and Baltic Sea.

The dependence of fitted A- and b-values on the WT was less pronounced as expected, especially the median values of A and b were within the same range. WTs with a lot of observations had a smaller difference between highest and lowest A- and b-value compared to WTs with a low number of observations. However, for some of these rare WTs only low R were measured, which indicates some kind of dependence on the WT. Aniol et al. (1980) also find a WT-dependence of the A- and b-values analysing measurements in South Germany. Similar to this study the A- and b-values of frequent WTs have a small difference. It is interesting to note that their weighted mean A-value is higher (256) and b-value is lower (1.42), respectively, compared to the values of this study. This indicates that in South Germany more large drops are measured. This is not surprising, because already Bringi et al. (2003) have shown that the mass-weighted mean drop size is larger for continental locations than for maritime locations. Hachani et al. (2017) find no strong dependence of the Z-R relationship on specific WTs, but on the rainfall types like stratiform and convective. This is supported by Kirsch et al. (2019) and other studies that show a clear difference of the A- and b-values for convective and stratiform rain. Frequent WTs might experience both, convective as well as stratiform rain, and the resulting A- and b-values represent an average condition. These relations indicate that probably no rain type is dominant for frequent WTs but for rare WTs. However, based on the results in this study it is not completely clear if the high (low) variability of some WTs is related to a low (high) number of observations or caused by different (same) and re-emerging DSD at the stations.

For all stations rain occurred in more than 90 % of the time, the percentage of snow was quite variable with lower percentages for stations at the North Sea coast. The dominance of rain is not surprising as temperature is mostly above freezing level. Lower temperatures at stations inland and continental influence related to advection from the east cause higher snow fractions for stations inland and at the coast of the Baltic Sea. Ice and hail are not so frequent as atmospheric conditions usually do not favour the formation of it (e.g. Punge and Kunz (2016)). Licznar and Krajewski (2016) find a similar fraction of mixed and hail analysing data from an Ott in Warsaw. However, it is unclear to which extend hail and ice particles were recorded correctly by the disdrometers. Pickering et al. (2019) mention some difficulties of the Thies to classify graupel.

The annual rainfall amount and rainfall kinetic energy (KE) had higher values in the eastern part of the North Sea compared to lower values in the western part of the North Sea and the Baltic Sea. The increase of rainfall amount from west to east across the North Sea is already mentioned by Tait et al. (1999) who analyse satellite rainfall data. The absolute values of the rainfall amount of the stations in Germany are in accordance with reported values of around 700 to 800 mm on the coast of the North Sea and 550 to 600 mm on the coast of the Baltic Sea (Deutscher Wetterdienst, 2020). Davison et al. (2005) estimate the monthly KE based on average daily rainfall data in England and Wales and find values between 375 and 625 $J\,m^{-2}$ for the area of Weybourne. These values give an annual value up to 7500 $J\,m^{-2}$, which is comparable to the calculated value in this study.

However, one could argue that the calculated KE is not the kinetic energy of drops that impact the turbine blade as only the measured fall velocity was used to calculate that. One of the challenges with calculating the actual impact velocity of the drops is that this velocity depends on the tip speed of the wind turbine which itself is a factor of the wind speed and the wind turbine type (Hasager et al., 2020). To calculate the impact velocity, the wind speed at hub-height and turbine operation including rotational speed and blade length are needed. Typical meteorological wind speed measurements on the ground do not represent correctly the wind speed at the turbine height as wind speed increases with increasing distance from the surface. At offshore locations, in situ meteorological data are not easy available. Letson et al. (2020) use wind speed from radars. Alternatively, modelled winds could be used for the offshore environment. In situ precipitation measurements with disdrometers are challenging offshore as there is hardly no infrastructure to install sensors and wind affects the registration of the particles. Regarding the latter, disdrometers can be optimized for these harsh conditions, for example by using an articulating disdrometer (Friedrich et al., 2013a) or a disdrometer with a cylindrical measurement volume (Klepp, 2015). Ideally though would be to combine blade speed from wind farm operation with the Z-R based KE information at wind farm sites to assess and predict LEE.

In general, by disregarding all precipitation types except rain for calculating the rainfall amount and the rainfall kinetic energy, both values might be slightly underestimated as rain of events with mixed precipitation is missing.

WTs with advection from NW and SW were dominating the precipitation probability as well as the annual rainfall amount and annual KE. That is not surprising as the weather is dominated by westerlies (Tait et al., 1999). Fernandez-Raga et al. (2016) and Fernández-Raga et al. (2020) also find high rain values for westerly directions in Spain. It is still part of ongoing research activities to investigate whether the annual rainfall amount, events with high rain rates or other rainfall parameters describe the influence of rain on LEE best. Assuming that the annual rainfall amount is the dominant criterion for LEE, than the most frequent WTs cause most damage. However, Hasager et al. (2020) stated that not only rain but also the wind climate has an influence on the development of LEE. Therefore, further analyses are needed to find out which WT causes most LEE.

6 Conclusion

The impact of precipitation particles cause degradation of the leading edge of wind turbine blades, better known as leading-edge erosion (LEE). To understand the role of precipitation on LEE better, we investigated the variation of relevant precipitation parameters with location and weather types (WTs). The focus was on analysing Z-R relationships and precipitation type as well as on annual rainfall amount and annual rainfall kinetic energy. As LEE seems to be more severe offshore, we chose the area of the North Sea and Baltic Sea with several wind farms installed as investigation area. As there are only limited offshore in situ precipitation measurements available, we focused on data from coastal stations.

We found that the variations of the A- and b-values of the Z-R relationship using all 1-minute measurements varied only slightly between the stations. This result supports our hypothesis that the mean microphysics and therefore drop-size distributions (DSD) at the stations are quite similar. The Z-R relationships fitted for specific WTs varied notable for some WTs. It is not clear if the WT or the low number of measurements for fitting the A- and b-value causes this higher variability. Hence, further research is needed on that. Furthermore, we showed that using WT-dependent Z-R relationships improve the estimation of R based on Z compared using the Marshall-Palmer values. The most frequent measured precipitation type was rain and drizzle, followed by snow. Other precipitation types like ice and hail were measured only for a few minutes each year. Our hypothesis was proved that the highest precipitation probability is associated to WTs with advection from NW or SW due the dominance of westerlies. The WT-dependence of snow was an exception as its probability was dominated by WTs with advection from the east and no prevailing advection. Annual values of rainfall amount and rainfall kinetic energy were higher for stations at the east coast of the North Sea and lower for stations close to the Baltic Sea and the west coast of the North Sea.

Assuming that the risk of erosion of the leading edges is governed by the cumulative rainfall amount or rainfall kinetic energy, wind farms in the eastern part of the North Sea have a higher risk than in the western part or in the Baltic Sea. As the number of large drops might also play a role in the development of LEE, the western part of the North Sea might also have a higher risk, because Weybourne had higher A-values for the Z-R relationship.

The demand of precipitation measurements offshore will increase, because more wind farms will be installed in the North Sea and Baltic Sea and an estimation of LEE risk probably gets more important. As in situ measurements are challenging due to frequently missing infrastructure, LEE relevant precipitation parameters could be calculated using Z-R relationships and annual values to estimate drop size and frequency of drop sizes.

Acknowledgements

We would like to thank DMI, DWD (P. Tracksdorf), NERC (B. Pickering) and UEA (G. Forster) for providing data. The main author likes to thank the EROSION project funded by the Innovation Fund Denmark grant 6154-00018B and DTU for funding. Furthermore, we are grateful to the comments of two anonymous reviewers.

7 Appendix 1

7.1 Quality control based on internal disdrometer data

All disdrometer data from the above mentioned stations undergone the steps listed in Table 2 to ensure that all non-precipitation related particles were filtered out.

Table 3 gives an overview about start and end date of the available time series, the disdrometer type, number of 1-minute intervals, percentage of missing 1-minute intervals as well as percentage of intervals that were disregarded by the quality control steps described in Table 2. No measurements were disregarded applying criteria QC1-7 and QC1-10 and therefore are not listed in Table 3. The percentage of missing values was above 20 % for the stations Bremerhaven, Horns Rev3, Hvide Sande, Thyborøn and Voulund. Additionally, the stations Horns Rev 3, Hvide Sande, Rodsand and Thyborøn showed a high percentage of measurements with a status problem and/or low laser amplitude. These four stations are located at offshore wind farms (Horns Rev 3, Rødsand) and at the west coast of Denmark (Hvide Sande, Thyborøn), respectively. The occurring harsh conditions

Table 2: Quality control of disdrometer data based on internal measured values of the disdrometers Thies LPM and Ott Parsivel[2]

Step	Argument	Description
QC1-1	Status	Status is different for Thies and Ott Ott has a parameter called "status". Only measurements with status 0 and 1 were accepted. Status of Thies was defined as a combination of laser and heating parameters (columns 116 to 144 in Telegram 5 according to manual of version 5.4110.xx.x00). If one of the parameters indicated an error, the measurement was disregarded. Special case station Weybourne: A Thies was installed, but the data provider introduced its own definition of data quality. Only data with quality flag equal to 1 was accepted.
QC1-2	Cumulative number of observed particles < 10	Measurements with less than 10 particles in 1 min were disregarded. Reference: Tokay and Bashor (2010)
QC1-3	Rain rate < 0.01 mm h^{-1}	Measurements with less than 0.01 mm h^{-1} in 1 min were disregarded. Reference: Tokay and Bashor (2010)
QC1-4	Data in less than 5 size-velocity combinations	Inspired by Ghada et al. (2018)
QC1-5	Negative SYNOP code	According to the Thies manual a negative SYNOP 4680 code indicates a sensor error. Such data was disregarded.
QC1-6	SYNOP code indicates unknown precipitation (41, 42)	According to the Thies manual, SYNOP 4680 code 41 and 42 characterize unknown precipitation and it is recommended not to use this data. Such data were disregarded.
QC1-7	Low measurement quality	Thies has a parameter called "measurement quality". Only data > 0 % to 100 % was accepted.
QC1-8	Sample interval is not 60 s	Ott has a parameter called sample interval due to use of DTU internal data collection software. Only data with a sample interval of 60 s (= 1 min) was accepted.
QC1-9	Rain rate > 500 mm h^{-1} in 1 min	Removal of implausible high 1-minute rain rates
QC1-10	Rainfall amount > 500 mm in 1 min	Removal of implausible high 1-minute rain amounts. Not checked for station Weybourne as no rain amount available.
QC1-11	Laser amplitude < 12000	According to Ott Helpdesk (personal communication), reliable measurements of Ott are related to laser amplitudes > 12000.

(e.g. high wind speeds and occurrence of sea salt on the protective glass of the laser) might caused problems. Therefore, it was decided to consider the following stations not for the further analysis: (i) Bremerhaven and Voulund (Ott), because of high percentage of missing 1-minute intervals and (ii) Horns Rev 3, Hvide Sande, Rødsand, Thyborøn because of multiple quality issues. Furthermore, station Risø was disregarded, because of the sheltered location of the disdrometer. Hence, only seven stations are used for further analyses.

7.2 Quality control of registered SYNOP code

The registered SYNOP codes of the remaining seven stations were validated, because the used algorithm by the manufacturer is unknown and we wanted to ensure that the registered SYNOP code is correct.

The SYNOP codes were merged into SYNOP groups. The reasons were: (i) SYNOP codes from Ott and Thies are not identically (e.g. intensity scale), (ii) SYNOP code from Ott does not agree with WMO SYNOP 4680 table (e.g. 88 is a reserved value in WMO SYNOP 4680 table, while used for soft hail in Ott manual). Therefore, following SYNOP groups covering following SYNOP codes:

- Rain/drizzle (henceforward rain): 51, 52, 53, 57, 58, 61, 62, 63
- Mixed rain/snow (henceforward mixed): 67, 68
- Snow: 71, 72, 73
- Ice: 74, 75, 76, 77, 88
- Hail: 89

To validate if the specific SYNOP group was registered correctly, the probability for snow, rain and mixed was calculated. That was done using method 3P2D published by Burdanowitz et al. (2016) using the variables temperature, relative humidity and 99th percentile of the drop diameter (T_rH_D99, T_rH_D99*). The temporal resolution of temperature and humidity data was 1 minute for Weybourne and 10 minute for Arkona, Fehrmarn, Helgoland, Marnitz and Norderney. In Voulund relative humidity was only available at 30-minute resolution, temperature was partly available at 10-minute interval, partly at 30-minute interval. For 10-minute and 30-minute interval data it was assumed that temperature and relative humidity did not change over 10 and 30 minutes, respectively. The 99th percentile of the drop diameter was calculated based on the quality controlled disdrometer data. Following Burdanowitz et al. (2016) we also applied temperature thresholds. No rain was possible for temperatures

Table 3: Start and end date of quality control time series. Number of 1-minute intervals, percentage of missing 1-minute intervals as well as percentage of disregarded 1-minute intervals based on quality control steps in Table 2. No measurements were disregarded applying criteria QC1-7 and QC1-10.

Station	Device	Start	End	# intervals	% missing	% Status (QC1-1)	% # drops (QC1-2)	% Low R (QC1-3)	% # channels (QC1-4)	% Neg. SYNOP (QC1-5)	% unkn. SYNOP (QC1-6)	% Sample i. (QC1-8)	% High R (QC1-9)	% laser amplitude (QC1-11)
Arkona	Thies LPM	2015-01-01 00:00	2018-12-31 23:59	1943185	0.89	0.03	12.62	1.25	0.03	3.80E-04	0.40	0	0	0
Bremerhaven	Thies LPM	2015-01-01 01:38	2018-12-31 23:59	2102960	20.09	0.02	10.23	1.02	0.01	8.08E-04	0.36	0	4.76E-05	0
Fehmarn	Thies LPM	2015-01-01 00:00	2018-12-31 23:59	2103840	0.84	0.00	9.44	1.32	0.03	1.76E-03	0.85	0	1.90E-04	0
Helgoland	Thies LPM	2015-10-01 00:00	2018-12-31 23:59	1501165	1.30	1.31	14.33	1.06	0.04	1.05E-03	0.19	0	0	0
Horns Rev 3	Ott Parsivel^2	2019-02-13 17:17	2020-02-04 08:12	512096	22.44	23.83	0.00	0.01	0	0	0	0.01	0	23.49
Hvide Sande	Ott Parsivel^2	2018-04-12 09:42	2019-10-01 14:21	773560	30.88	30.52	0.01	0.02	1.29E-04	0	0	0.03	0	13.85
Marnitz	Thies LPM	2015-01-01 00:00	2018-12-31 23:59	2103840	2.02	0.00	8.90	1.70	0.01	4.75E-04	0.37	0	0	0
Norderney	Thies LPM	2015-01-01 00:00	2019-01-01 00:00	1812145	1.73	0.48	13.50	1.40	0.03	1.43E-03	0.17	0	1.43E-04	0
Risø	Ott Parsivel^2	2018-03-22 15:53	2020-05-31 23:01	979629	9.15	1.92	0.10	0.08	1.82E-03	0	0	0.63	0	1.22
Rødsand	Ott Parsivel^2	2018-12-11 09:20	2020-03-19 17:20	668641	4.65	9.44	0.05	0.09	5.98E-04	0	0	0.88	0	19.80
Thyborøn	Ott Parsivel^2	2018-05-04 11:33	2019-10-01 14:22	741770	46.73	14.60	0.00	0.01	0	0	0	0.03	0	8.27
Voulund	Thies LPM	2012-02-09 11:44	2018-02-27 12:23	3045498	5.52	0.06	9.65	2.05	0.03	0.02	0.03	0	3.28E-05	0
Voulund (Ott)	Ott Parsivel^2	2018-01-31 12:22	2019-10-01 14:24	875643	32.74	0.85	0.01	0.03	5.71E-04	0	0	0.04	0	3.93
Weybourne	Thies LPM	2017-02-10 00:00	2019-09-30 23:59	1386720	12.96	0.02	12.93	1.08	0.04	0.01	1.74	0	0	0

below −6 °C and no snow was possible for temperatures above +8 °C. In case the registered SYNOP group was unequal to the SYNOP group with the highest probability, the registered SYNOP group was changed to the one with the highest probability. For example: In case the registered SYNOP group was snow but the probability of rain was higher, the registered SYNOP group was changed to rain. Possible changes were snow → rain, snow → mixed, rain → snow, rain → mixed, mixed → snow, mixed → rain.

The quality control of the SYNOP groups ice and hail was more difficult. In general, different precipitation types can occur at the same time. However, automatic devices like disdrometers only store the highest SYNOP code (Merenti-Välimäki et al., 2001). Hence, it is possible that different types occur at the same time (e.g. hail and rain). Furthermore, the SYNOP group ice includes ice pellets, ice crystals and soft hail. As the algorithm for the SYNOP code detection of both disdrometer sensors is not known, it is not clear under which conditions these precipitation types were registered. For example snow can have different forms depending for example on the temperature and the melting status of the snowflake (Yuter et al., 2006; Ishizaka et al., 2013) and some of the ice particles might be registered during snowfall. Therefore, following approach was chosen: In case the probability of snow or mixed was higher than for rain, the SYNOP group ice or hail was reclassified to snow or mixed. The SYNOP group snow might be a bit less strictly defined by such a reclassification, but in context of LEE we were interested in events with hail or ice (in co-existence with rain). Possible changes were ice → snow, ice → mixed, hail → snow, hail → mixed. The percentages of reclassification were low, the maximum was 0.25 % (5438 intervals) for the station Norderney for the reclassification mixed → rain. These low reclassification fractions are in line with Fehlmann et al. (2020) who find a satisfying classification of rain and snow for Thies.

7.3 Quality control of SYNOP group rain/drizzle

For the calculation of rainfall kinetic energy, reflectivity and rain rate only data of the SYNOP group rain was used. The size-velocity histograms showed that still suspicious particles, e.g. particles with very low or high fall velocity, were part of the rain dataset. The source of these particles was not clear. It could be possible that they were caused for example by the breakup at the housing of the sensor or drops in spider webs. Suspicious particles were disregarded by processing following two steps:

- QC3-1: Particles with a diameter > 8 mm were disregarded, because raindrops with larger diameter breakup due to hydrodynamic instability (Jones et al., 2010).

Table 4: Fitted A-values of the Z-R relationship for all stations and weather types (WTs).

Weather type	Arkona	Fehmarn	Helgoland	Marnitz	Norderney	Voulund	Weybourne
all WTs	196	191	201	164	202	182	233
XXAAD	189	181	179	203	125	244	201
NEAAD	366	2997	48	118	80	225	699
SEAAD							172
SWAAD	167	150	154	194	188	209	332
NWAAD	169	187	225	156	199	155	204
XXAAW	232	230	170	158	228	148	236
NEAAW	55			38	221	155	
SEAAW							21
SWAAW	171	232	198	172	170	168	259
NWAAW	171	172	181	145	152	142	190
XXACD	82	179	247	247	161	267	255
NEACD	176	314	577	61	232	234	321
SEACD							
SWACD	248	221	221	220	232	180	171
NWACD	144	155	219	170	190	226	208
XXACW	247	255	287	143	364	174	489
NEACW							
SEACW							
SWACW	166	164	147	124	181	185	233
NWACW	208	194	169	110	312	181	132
XXCAD		171		278	242	167	346
NECAD							
SECAD							396
SWCAD	196	254	194	317	249	220	224
NWCAD	286	188	383	128	54	159	
XXCAW		252	112		294	147	117
NECAW							
SECAW	338	173	157		154	192	390
SWCAW	265	214	221	177	190	207	230
NWCAW	309	288	121	128	98	235	372
XXCCD	173	220	178	231	206	203	268
NECCD	168	145	186	231	102	234	616
SECCD	227	74		395	596	178	478
SWCCD	339	195	198	173	200	118	203
NWCCD	335	192	177	225	277	168	111
XXCCW	187	230	209	201	192	226	187
NECCW		194		255			
SECCW	232	174	126	345	131	181	226
SWCCW	193	173	210	168	216	198	261
NWCCW	242	221	125	170	228	292	222

- QC3-2: Drops with a fall velocity > +/− 60 % of the terminal fall velocity calculated with Atlas et al. (1973) were disregarded. This quality criterion is based on Friedrich et al. (2013b).

While the number of disregarded drops due to QC3-1 was low, QC3-2 lead to a notable high number of disregarded drops. Stations equipped with a Thies, the percentages were quite high with values between 45 % (Arkona) and 54 % (Norderney). Most of the disregarded drops had a diameter < 2 mm.

8 Appendix 2

Result of fitted A- and b-values are in Table 4 and Table 5.

Table 5: Fitted b-values of the Z-R relationship for all stations and weather types (WTs).

Weather type	Arkona	Fehmarn	Helgoland	Marnitz	Norderney	Voulund	Weybourne
all WTs	1.77	1.83	1.74	1.79	1.84	1.88	1.85
XXAAD	1.51	2.08	1.58	1.96	2.32	2.02	2.59
NEAAD	2.22	3.15	1.29	2.15	1.84	1.97	2.54
SEAAD							1.66
SWAAD	1.72	2.03	2.14	1.73	2.11	1.93	1.68
NWAAD	1.87	1.80	1.63	1.87	2.04	2.17	2.15
XXAAW	1.89	1.63	1.64	1.88	1.74	1.97	1.48
NEAAW	1.37			1.30	2.46	2.35	
SEAAW							1.21
SWAAW	1.73	1.65	1.71	1.82	1.86	2.00	1.75
NWAAW	2.05	1.89	1.88	1.81	2.05	2.17	2.08
XXACD	2.12	1.62	1.69	1.82	2.09	1.66	2.28
NEACD	1.95	1.75	2.49	1.90	1.68	1.94	1.82
SEACD							
SWACD	1.61	1.84	1.65	1.76	1.85	1.85	2.01
NWACD	1.86	2.00	1.72	1.75	1.95	1.73	1.84
XXACW	1.81	2.32	1.26	1.71	1.78	1.94	1.89
NEACW							
SEACW							
SWACW	2.03	1.70	1.82	1.84	1.66	1.83	1.81
NWACW	1.72	1.89	1.77	1.97	1.77	1.99	2.16
XXCAD		1.70		2.13	2.54	2.18	1.90
NECAD							
SECAD							3.06
SWCAD	1.88	1.64	1.93	2.08	2.08	1.66	1.88
NWCAD	2.44	2.26	1.44	2.24	2.54	2.39	
XXCAW		1.75	1.95		1.75	1.88	2.18
NECAW							
SECAW	1.57	1.86	2.05		2.22	1.68	1.65
SWCAW	1.65	1.79	1.68	1.78	1.97	1.76	1.85
NWCAW	1.78	1.90	2.00	1.91	2.29	1.47	2.04
XXCCD	1.90	1.75	1.93	1.93	1.59	1.69	1.82
NECCD	1.62	1.74	2.01	2.12	1.51	2.00	2.34
SECCD	1.78	2.55		2.29	1.42	2.25	1.98
SWCCD	1.46	1.96	1.87	2.38	2.03	2.16	1.83
NWCCD	1.69	1.86	1.76	2.03	1.72	2.29	2.34
XXCCW	2.18	1.59	2.28	1.63	1.73	1.77	1.69
NECCW		1.45		1.74			
SECCW	1.69	1.74	1.91	1.42	1.61	1.78	1.82
SWCCW	1.81	1.86	1.68	1.73	1.88	1.82	1.85
NWCCW	1.91	1.92	2.23	2.04	1.99	1.57	2.10

References

Adirosi, E., N. Roberto, M. Montopoli, E. Gorgucci, L. Baldini, 2018: Influence of Disdrometer Type on Weather Radar Algorithms from Measured DSD: Application to Italian Climatology. – Atmosphere **9**, 360. DOI:10.3390/atmos9090360.

Alfieri, L., P. Claps, F. Laio, 2010: Time-dependent Z-R relationships for estimating rainfall fields from radar measurements. – Nat. Hazards Earth Syst. Sci. **10**, 149–158. DOI:10.5194/nhess-10-149-2010.

Angulo-Martínez, M., S. Beguería, B. Latorre, M. Fernández-Raga, 2018: Comparison of precipitation measurements by OTT Parsivel2 and Thies LPM optical disdrometers. – Hydrol. Earth Syst. Sci. **22**, 2811–2837. DOI:10.5194/hess-22-2811-2018.

Aniol, R., J. Riedl, M. Dieringer, 1980: Über kleinräumige und zeitliche Variationen der Niederschlagsintensität. – Meteorol. Rdsch. **33**, 50–56.

Atlas, D., R.C. Srivastava, R.S. Sekhon, 1973: Doppler radar characteristics of precipitation at vertical incidence. – Rev. Geophys. **11**, 1–35. DOI:10.1029/RG011i001p00001.

Bandy, B., 2002: Weybourne Atmospheric Observatory: Longterm Meteorological Measurements 2002-Present. NCAS British Atmospheric Data Centre. 1 p., Available at: https://catalogue.ceda.ac.uk/uuid/6013826d522b4682823f757f9244e6c3 (Accessed: April 15, 2020).

Bech, J.I., C.B. Hasager, C. Bak, 2018: Extending the life of wind turbine blade leading edges by reducing the tip speed during extreme precipitation events. – Wind Energ. Sci. **3**, 729–748. DOI:10.5194/wes-3-729-2018.

Bissolli, P., E. Dittmann, 2001: The objective weather type classification of the German Weather Service and its possibilities of application to environmental and meteorological investigations. – Meteorol. Z. **10**, 253–260. DOI:10.1127/0941-2948/2001/0010-0253.

Bringi, V.N., V. Chandrasekar, J. Hubbert, E. Gorgucci, W.L. Randeu, M. Schoenhuber, 2003: Raindrop Size Distribution in Different Climatic Regimes from Disdrometer and Dual-Polarized Radar Analysis. – J. Atmos. Sci. **60**, 354–365. DOI:10.1175/1520-0469(2003)060%3C0354:RSDIDC%3E2.0.CO;2.

Bumke, K., J. Seltmann, 2012: Analysis of Measured Drop Size Spectra over Land and Sea. – ISRN Meteorology **2012**, 1–10. DOI:10.5402/2012/296575.

Burdanowitz, J., C. Klepp, S. Bakan, 2016: An automatic precipitation-phase distinction algorithm for optical disdrometer data over the global ocean. – Atmos. Meas. Tech. **9**, 1637–1652. DOI:10.5194/amt-9-1637-2016.

Davison, P., M.G. Hutchins, S.G. Anthony, M. Betson, C. Johnson, E.I. Lord, 2005: The relationship between potentially erosive storm energy and daily rainfall quantity in England and Wales. – Sci. Total Env. **344**, 15–25. DOI:10.1016/j.scitotenv.2005.02.002.

Deutscher Wetterdienst, 2020: Klimastatusbericht Deutschland Jahr 2019. – DWD, Geschäftsbereich Klima und Umwelt, 23 p., Available at: https://www.dwd.de/DE/leistungen/klimastatusbericht/publikationen/ksb_2019.pdf?__blob=publicationFile&v=5 (Accessed: August 24, 2020).

Doelling, I.G., J. Joss, J. Riedl, 1998: Systematic variations of Z-R-relationships from drop size distributions measured in northern Germany during seven years. – Atmos. Res. **47–48**, 635–649. DOI:10.1016/S0169-8095(98)00043-X.

Fehlmann, M., M. Rohrer, A. von Lerber, M. Stoffel, 2020: Automated precipitation monitoring with the Thies disdrometer: biases and ways for improvement. – Atmos. Meas. Tech. **13**, 4683–4698. DOI:10.5194/amt-13-4683-2020.

Fernandez-Raga, M., A. Castro, E. Marcos, C. Palencia, R. Fraile, 2016: Weather types and rainfall microstructure in Leon, Spain. – Int. J. Climatol. **37**, 1834–1842. DOI:10.1002/joc.4816.

Fernández-Raga, M., R. Fraile, C. Palencia, E. Marcos, A.M. Castañón, A. Castro, 2020: The Role of Weather Types in Assessing the Rainfall Key Factors for Erosion in Two Different Climatic Regions. – Atmosphere **11**, 443. DOI:10.3390/atmos11050443.

Frasson, R.P. de M., L.K. da Cunha, W.F. Krajewski, 2011: Assessment of the Thies optical disdrometer performance. – Atmos. Res. **101**, 237–255. DOI:10.1016/j.atmosres.2011.02.014.

Freeman, K., C. Frost, G. Hundleby, A. Roberts, B. Valpy, H. Holttinen, L. Ramírez, I. Pineda, 2019: Our Energy, Our Future – How Offshore Wind Will Help Europe Go Carbon-Neutral. – WindEurope, 80 p., Available at: https://windeurope.org/wp-content/uploads/files/about-wind/reports/WindEurope-Our-Energy-Our-Future.pdf (Accessed: September 17, 2020).

Friedrich, K., S. Higgins, F.J. Masters, C.R. Lopez, 2013a: Articulating and Stationary PARSIVEL Disdrometer Measurements in Conditions with Strong Winds and Heavy Rainfall. – J. Atmos. Oceanic Technol. **30**, 2063–2080. DOI:10.1175/JTECH-D-12-00254.1.

Friedrich, K., E.A. Kalina, F.J. Masters, C.R. Lopez, 2013b: Drop-Size Distributions in Thunderstorms Measured by Optical Disdrometers during VORTEX2. – Mon. Wea. Rev. **141**, 1182–1203. DOI:10.1175/MWR-D-12-00116.1.

Ghada, W., A. Buras, M. Lüpke, C. Schunk, A. Menzel, 2018: Rain Microstructure Parameters Vary with Large-Scale Weather Conditions in Lausanne, Switzerland. – Remote Sens. **10**, 811. DOI:10.3390/rs10060811.

Hachani, S., B. Boudevillain, G. Delrieu, Z. Bargaoui, 2017: Drop Size Distribution Climatology in Cévennes-Vivarais Region, France. – Atmosphere **8**, 233. DOI:10.3390/atmos8120233.

Hasager, C., F. Vejen, J.I. Bech, W.R. Skrzypiński, A.-M. Tilg, M. Nielsen, 2020: Assessment of the rain and wind climate with focus on wind turbine blade leading edge erosion rate and expected lifetime in Danish Seas. – Renew. Energ. **149**, 91–102. DOI:10.1016/j.renene.2019.12.043.

Hidalgo, J., R. Jougla, 2018: On the use of local weather types classification to improve climate understanding: An application on the urban climate of Toulouse. – PLoS ONE **13**, e0208138. DOI:10.1371/journal.pone.0208138.

Ignaccolo, M., C. De Michele, 2020: One, No One, and One Hundred Thousand: The Paradigm of the *Z–R* Relationship. – J. Hydrometeorol. **21**, 1161–1169. DOI:10.1175/JHM-D-19-0177.1.

Ishizaka, M., H. Motoyoshi, S. Nakai, T. Shiina, T. Kumakura, K. Muramoto, 2013: A New Method for Identifying the Main Type of Solid Hydrometeors Contributing to Snowfall from Measured Size-Fall Speed Relationship. – J. Meteor. Soc. Jpn. **91**, 747–762. DOI:10.2151/jmsj.2013-602.

Johannsen, L.L., N. Zambon, P. Strauss, T. Dostal, M. Neumann, D. Zumr, T.A. Cochrane, G. Blöschl, A. Klik, 2020: Comparison of three types of laser optical disdrometers under natural rainfall conditions. – Hydrol. Sci. J. **65**, 524–535. DOI:10.1080/02626667.2019.1709641.

Jones, B.K., J.R. Saylor, F.Y. Testik, 2010: Raindrop morphodynamics. – In: Testik F.Y., M. Gebremichael (eds.): Rainfall: State of the Science. – Geophys. Monograph **191**, American Geophysical Union, 7–28. DOI:10.1029/GM191.

Keegan, M.H., D.H. Nash, M.M. Stack, 2013: On erosion issues associated with the leading edge of wind turbine blades. – J. Phys. D: Appl. Phys. **46**, 383001. DOI:10.1088/0022-3727/46/38/383001.

Kirsch, B., M. Clemens, F. Ament, 2019: Stratiform and Convective Radar Reflectivity–Rain Rate Relationships and Their Potential to Improve Radar Rainfall Estimates. – J. Appl. Meteor. Climatol. **58**, 2259–2271. DOI:10.1175/JAMC-D-19-0077.1.

Klepp, C., 2015: The oceanic shipboard precipitation measurement network for surface validation – OceanRAIN. – Atmos. Res. **163**, 74–90. DOI:10.1016/j.atmosres.2014.12.014.

Klepp, C., S. Michel, A. Protat, J. Burdanowitz, N. Albern, M. Kähnert, A. Dahl, V. Louf, S. Bakan, S.A. Buehler, 2018: OceanRAIN, a new in-situ shipboard global ocean surface-reference dataset of all water cycle components. – Sci Data **5**, 180122. DOI:10.1038/sdata.2018.122.

Krajewski, W.F., J.A. Smith, 1991: On the Estimation of Climatological Z-R Relationships. – Journal of Applied Meteorology **30**, 1436–1445. DOI:10.1175/1520-0450(1991)030%3C1436:OTEOCR%3E2.0.CO;2.

Kruger, A., W.F. Krajewski, 2002: Two-Dimensional Video Disdrometer: A Description. – J. Atmos. Oceanic Technol. **19**, 16.

Letson, F., R.J. Barthelmie, S.C. Pryor, 2020: Radar-derived precipitation climatology for wind turbine blade leading edge erosion. – Wind Energ. Sci. **5**, 331–347. DOI:10.5194/wes-5-331-2020.

Licznar, P., W.F. Krajewski, 2016: Precipitation Type Specific Radar Reflectivity-rain Rate Relationships for Warsaw, Poland. – Acta Geophysica **64**, 1840–1857. DOI:10.1515/acgeo-2016-0071.

Linderson, M.-L., 2001: Objective classification of atmospheric circulation over southern Scandinavia. – Int. J. Climatol. **21**, 155–169. DOI:10.1002/joc.604.

Macdonald, H., D. Infield, D.H. Nash, M.M. Stack, 2016: Mapping hail meteorological observations for prediction of erosion in wind turbines: UK hail meteorological observations. – Wind Energy **19**, 777–784. DOI:10.1002/we.1854.

Marshall, J.S., W.M.K. Palmer, 1948: The distribution of raindrops with size. – J. Meteor. **5**, 165–166. DOI:10.1175/1520-0469(1948)005<0165:TDORWS>2.0.CO;2.

Marshall, J.S., W. Hitschfeld, K.L.S. Gunn, 1955: Advances in Radar Weather. – In: Adv. Geophys. **2**, Elsevier, 1–56. DOI:10.1016/S0065-2687(08)60310-6.

Merenti-Välimäki, H.-L., J. Lönnqvist, P. Laininen, 2001: Present weather: comparing human observations and one type of automated sensor. – Meteor. Apps **8**, 491–496. DOI:10.1017/S1350482701004108.

Mishnaevsky, L., 2019: Repair of wind turbine blades: Review of methods and related computational mechanics problems. – Renew. Energ. **140**, 828–839. DOI:10.1016/j.renene.2019.03.113.

Natural Environment Research Council, Met Office, B.S. Pickering, R. Neely III, D. Harrison, 2019: The Disdrometer Verification Network (DiVeN): particle diameter and fall velocity measurements from a network of Thies Laser Precipitation Monitors around the UK (2017–2019). – CEDA Archive. DOI:10.5285/602f11d9a2034dae9d0a7356f9aeaf45.

Petrů, J., J. Kalibová, 2018: Measurement and computation of kinetic energy of simulated rainfall in comparison with natural rainfall. – Soil Water Res. **13**, 226–233. DOI:10.17221/218/2016-SWR.

Pickering, B.S., R.R. Neely III, D. Harrison, 2019: The Disdrometer Verification Network (DiVeN): a UK network of laser precipitation instruments. – Atmos. Meas. Tech. **12**, 5845–5861. DOI:10.5194/amt-12-5845-2019.

Piotrowicz, K., D. Ciaranek, 2020: A selection of weather type classification systems and examples of their application. – Theor. Appl. Climatol **140**, 719–730. DOI:10.1007/s00704-020-03118-2.

Punge, H.J., M. Kunz, 2016: Hail observations and hailstorm characteristics in Europe: A review. – Atmos. Res. **176–177**, 159–184. DOI:10.1016/j.atmosres.2016.02.012.

R Core Team, 2020: R: A Language and Environment for Statistical Computing. – R Foundation for Statistical Computing, Vienna, Austria. Available at: https://www.R-project.org/.

Raupach, T.H., A. Berne, 2015: Correction of raindrop size distributions measured by Parsivel disdrometers, using a two-dimensional video disdrometer as a reference. – Atmos. Meas. Tech. **8**, 343–365. DOI:10.5194/amt-8-343-2015.

Sareen, A., C.A. Sapre, M.S. Selig, 2014: Effects of leading edge erosion on wind turbine blade performance: Effects of leading edge erosion. – Wind Energy **17**, 1531–1542. DOI:10.1002/we.1649.

Seo, D.-J., A. Seed, G. Delrieu, 2010: Radar and multisensor rainfall estimation for hydrologic applications. – In: Testik, F.Y., M. Gebremichael (Eds.): Rainfall: State of the Science. – Geophys. Monograph **191**, American Geophysical Union, 79–104. DOI:10.1029/2010GM000952.

Slot, H.M., E.R.M. Gelinck, C. Rentrop, E. van der Heide, 2015: Leading edge erosion of coated wind turbine blades: Review of coating life models. – Renew. Energ. **80**, 837–848. DOI:10.1016/j.renene.2015.02.036.

Tait, A.B., E.C. Barrett, M.J. Beaumont, P.A. Brown, M.J. Taberner, M.C. Todd, 1999: Interpretation of an atlas of passive microwave-derived rainfall over the eastern North Atlantic Ocean and North Sea. – Int. J. Climatol. **19**, 231–252.

Tilg, A.-M., F. Vejen, C.B. Hasager, M. Nielsen, 2020: Rainfall Kinetic Energy in Denmark: Relationship with Drop Size, Wind Speed, and Rain Rate. – J. Hydrometeorol. **21**, 1621–1637. DOI:10.1175/JHM-D-19-0251.1.

Tokay, A., P.G. Bashor, 2010: An Experimental Study of Small-Scale Variability of Raindrop Size Distribution. – J. Appl. Meteor. Climatol. **49**, 2348–2365. DOI:10.1175/2010JAMC2269.1.

Ulbrich, C.W., D. Atlas, 1998: Rainfall Microphysics and Radar Properties: Analysis Methods for Drop Size Spectra. – J. Appl. Meteor. **37**, 912–923.

Verma, A.S., S.G.P. Castro, Z. Jiang, J.J.E. Teuwen, 2020: Numerical investigation of rain droplet impact on offshore wind turbine blades under different rainfall conditions: A parametric study. – Compos Struct. **241**, 112096. DOI:10.1016/j.compstruct.2020.112096.

Verrier, S., L. Barthès, C. Mallet, 2013: Theoretical and empirical scale dependency of Z-R relationships: Evidence, impacts, and correction. – J. Geophys. Res. Atmos. **118**, 7435–7449. DOI:10.1002/jgrd.50557.

Wang, P.K., 2013: Physics and Dynamics of Clouds and Precipitation. – Cambridge University Press, 452 pp.

Yuter, S.E., D.E. Kingsmill, L.B. Nance, M. Löffler-Mang, 2006: Observations of Precipitation Size and Fall Speed Characteristics within Coexisting Rain and Wet Snow. – J. Appl. Meteor. Climatol. **45**, 1450–1464. DOI:10.1175/JAM2406.1.

Zambon, N., L. Lolk Johannsen, P. Strauss, T. Dostal, D. Zumr, M. Neumann, T.A. Cochrane, A. Klik, 2020: Rainfall Parameters Affecting Splash Erosion under Natural Conditions. – Appl. Sci. **10**, 4103. DOI:10.3390/app10124103.